Adhesion and Particle Deformation of Submicron-Sized Latex Particles on Hydrophobically Modified Solid Substrates at Room Temperature

Jung Min Lee and Jung Hyun Kim*

Department of Chemical Engineering, Yonsei University, 134 Shinchon-Dong, Seodaemoon-Gu, Seoul 120-749, Republic of Korea

In Woo Cheong

Department of Applied Chemistry, Kyungpook National University, 1370 Sankyuk-dong, Buk-gu, Daegu 702-701, Republic of Korea

Chee Cheong Ho

Institute Kimia Malaysia, 127B Jalan Aminuddin Baki, Taman Tun Dr Ismail, 60000 Kuala Lumpur, Malaysia

Received October 13, 2007; Revised Manuscript Received January 7, 2008

ABSTRACT: Two- and three-dimensional colloid arrays were fabricated using three different kinds of monodisperse poly(styrene/sodium *p*-styrenesulfonate) (poly(St/NaSS) (i.e., high- and low-charged un-cross-linked, and low-charged cross-linked poly(St/NaSS) particles) on 3-aminopropyltrimethoxysilane (APTMS)-modified glass substrates at 20 °C. The array patterns were investigated by field-emission scanning electron microscopy (SEM), atomic force microscopy (AFM), and UV−vis spectroscopic analyses. The adhesive force measured by AFM analysis revealed negligible attractive force between APTMS and the poly(St/NaSS) particles. The adhesion force measured between a 3-aminopropyltrimethoxysilane (APTMS)-modified SiN_x tip and the self-assembled particle arrays was in good agreement with the attractive force calculated using the Lifshitz theory with the appropriate Hamaker constants. The cross-linked poly(St/NaSS) particles on the APTMS-modified glass substrate showed mainly hexagonal and square-lattice-free patterns without any crevices, in stark contrast to that of the cleaned, bare glass substrate. The APTMS layer provided the necessary "free-slipping" condition in which nuclei of scattered pinnings of particles in the colloidal crystal were absent. As a consequence, dense fcc (or hcp) packing densities (high-charged un-cross-linked: 0.80; low-charged un-cross-linked: 0.76; low-charged cross-linked: 0.76) and narrower stop bands were obtained.

Introduction

Colloid science includes an extremely broad range of diverse fields. Colloidal particles have been used as major components of diverse industrial products such as inks, coatings, paints, papers, cosmetics, and rheological fluids.[1] In particular, two- and three-dimensional (2- and 3-D) periodic structures of monodisperse colloidal particles are versatile and used as microlenses, templates for optical filters, microporous membranes, photonic materials, sensors, and optical filters.[1−9] Monodisperse latex particles are known to undergo ordering to form a colloidal crystalline phase with a hexagonal closed packing structure at low ionic strength when the repulsion between the particles is strong.[10] Similar periodic order and hexagonal closed-packed particles in 2-D arrays of the latex films have been reported previously by Winnik and co-workers.[11] Recently, photonic crystals for the visible range have been prepared mostly by self-assembly of polymer colloids of several hundred nanometers in diameter, which were dried and crystallized into a face-centered-cubic lattice.[12−14]

To fabricate high-quality crystals on a solid substrate, it is very important to understand the interactions between the colloidal particles and substrate.[15−18] The mechanism of the formation of 2- and 3-D crystals from latex particles on hydrophobically modified glass substrates has been reported previously.[19] It demonstrated that the adhesional deformation of particles by strong attractive capillary forces, the convective transport of particles toward the ordered region, and the "free-slipping" condition attributable to the hydrophobic hairy chain layers of the 3-aminopropyltrimethoxysilane (APTMS) were main factors governing the qualities of ordering of the particle arrays.[19] However, the evidence that the APTMS layer provided the "free-slipping" condition important in ensuring formation of defect-free colloidal crystals is yet to be fully confirmed. Thus, this calls for further investigation in greater details of the interaction between the APTMS layer and the various poly(St/NaSS) colloidal particles, including adhesional deformation.

Knowledge of the interaction between colloidal particles and a surface is a precondition in understanding the adhesional phenomenon since the macroscopic behavior of particulates at the surface of a substrate is inextricably linked to the microscopic details of the interactions between them. In this study, we evaluated the Lifshitz−London−van der Waals attractive force between the particles and the substrate and compared this with the directly measured force−displacement curve and the pull-off force using atomic force microscopy.[20] The adhesional force between an AFM tip and a sample surface generally consists of the van der Waals force, electrostatic force, chemical bonding force, and capillary force.[21]

* Corresponding author: Tel +82 2 2123 7633; Fax +82 2 312 0305; e-mail jayhkim@yonsei.ac.kr.

10.1021/ma702283a CCC: $40.75
Published on Web 02/27/2008

Table 1. Characteristics of the High-Charge Un-Cross-Linked (HCU), Low-Charge Un-Cross-Linked (LCU), and Low-Charge Cross-Linked (LCC) Monodisperse Poly(St/NaSS) Latex Particles

sample ID	solid content/wt %	$\overline{D_n}$/nm	$\overline{D_w}$/nm	PDI[a]	surface charge density (σ)[b]/μC cm^{-2}	cross-linking content[c]/%
HCU	7.8	235	236.6	1.007	38	
LCU	8.3	242	243.7	1.007	3	
LCC	7.9	228	229.6	1.007	4	92.8

[a] PDI = $\overline{D_w}/\overline{D_n}$, $\overline{D_w}$, and $\overline{D_n}$ were measured by capillary hydrodynamic fractionation (CHDF). [b] The surface charge density was measured by titration method with 0.02 M NaOH aqueous solutions under a N_2 atmosphere. [c] Cross-linking content was measured by the Soxhlet extraction technique.

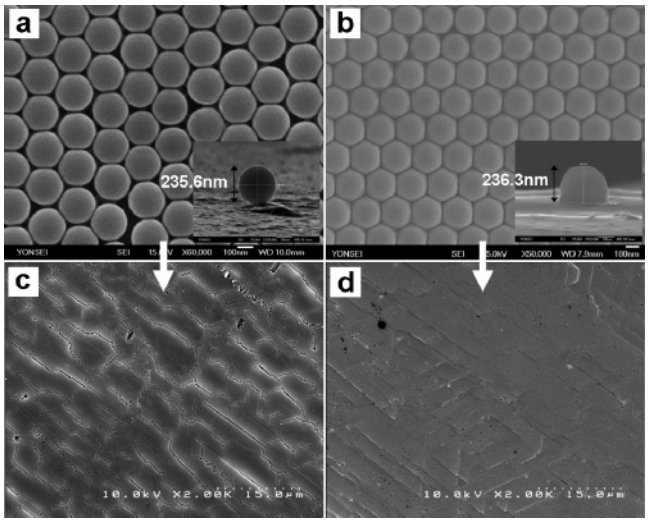

Figure 1. FE-SEM micrographs of colloidal crystals of HCU (diameter 235 nm) poly(St/NaSS) particles: (a) and (b) are top view of monolayer at high magnification (×60 000 (a) and ×50 000 (b)) (insets: 85° tilted view of individual particles); (c) and (d) are top view of multilayer at low magnification (×2000); (a) and (c) are on cleaned, bare glass substrate; (b) and (d) are on APTMS-modified glass substrate at 20 °C.

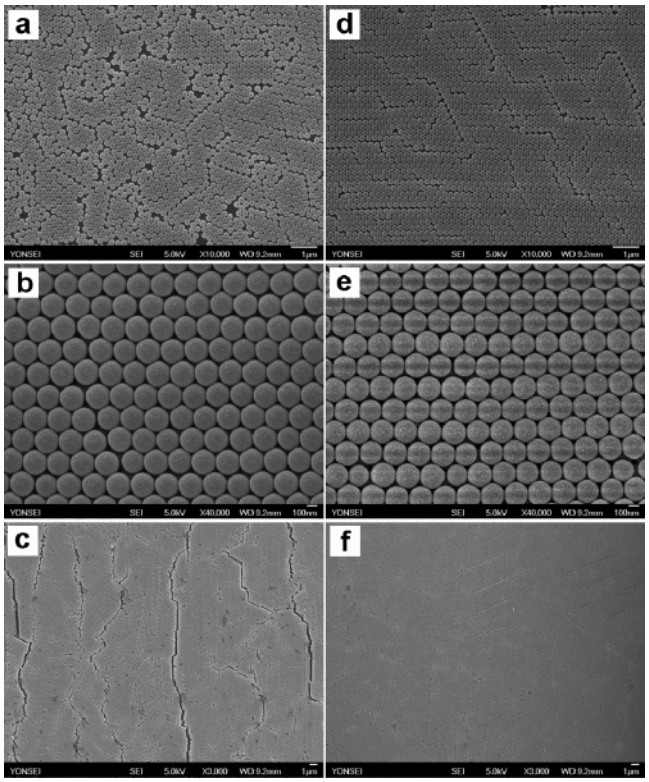

Figure 2. FE-SEM micrographs of colloidal crystals of LCC (diameter 228 nm) poly(St/NaSS) particles: (a) and (d) are top view of monolayer at high magnification (×10 000); (b) and (e) are top view of multilayer at high magnification (×40 000); (c) and (f) are top view of multilayer at low magnification (×3000); (a) to (c) are on the cleaned, bare glass substrate; (d) to (f) are on the APTMS-modified glass substrate at 20 °C.

Since the adhesion between surfaces is governed by deformation and the surface forces acting between them depends on their geometry, the attractive force between (1) a hard sphere and a hard planar surface and (2) two interacting hard spheres across a medium were calculated. The effects of particle surface charge, particle hardness, and the hydrophobicity of the substrates on attractive force between the substrate and the particles, and array patterns and packing were investigated. These are believed to be critical factors in minimizing defects in photonic crystal formation.

Experimental Section

Materials. Styrene monomer (St, Junsei, Japan) was purchased and purified using an inhibitor remover column (Aldrich). The purified monomer was kept at −5 °C until use. Sodium *p*-styrenesulfonate (NaSS, Aldrich) and divinylbenzene (DVB, Aldrich) were purchased and used as received. Potassium persulfate (KPS, Junsei, Japan) was recrystallized with methanol, dried in a vacuum oven, and kept at −5 °C until use. Sodium bicarbonate ($NaHCO_3$), 3-aminopropyltrimethoxysilane (APTMS), and anhydrous methanol were analytical grades and used without further purification. Double-distilled and deionized (DDI) water was used throughout the experiment.

Preparation of Monodisperse Poly(St/NaSS) Latex Particles. High-charge un-cross-linked (HCU), low-charge un-cross-linked (LCU), and low-charge cross-linked (LCC) poly(St/NaSS) latex particles were prepared by emulsifier-free emulsion polymerization using a two-stage shot-growth method at 70 °C.[22,23] Emulsifier-free emulsion polymerizations of styrene were carried out in a 500 mL double-jacketed glass reactor equipped with a reflux condenser, a nitrogen gas inlet, an ingredient inlet, an initiator funnel, and a mechanical stirrer. The reaction temperature and the stirring rate were 50 °C and at 400 rpm, respectively. In the first stage of the polymerization, a small amount (0.24 mM) of NaSS was added to control the polydispersity and particle size. A second-stage shot of the monomer mixture (19.2 mM of styrene and 2.4 mM of NaSS)

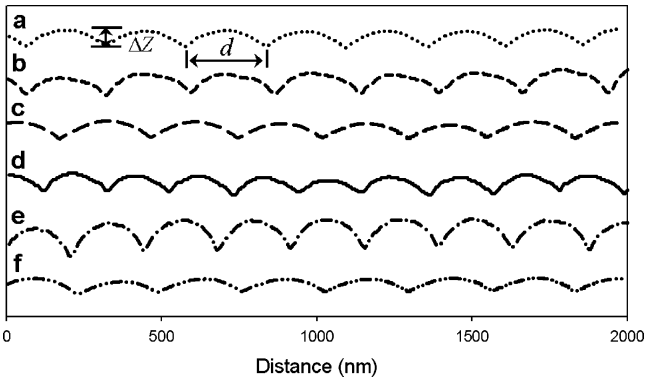

Figure 3. AFM tracing of the *z*-axis profiles of HCU (a and d), LCU (b and e), and LCC (c and f) poly(St/NaSS) particles on cleaned, bare glass substrate (a−c) and on the APTMS-modified glass substrates (d−f). The nomenclatures for ΔZ and d are given in Table 2.

Table 2. Peak-to-Valley Data of the Cross Sections of the HCU (a and d) and LCU (b and e) Poly(St/NaSS) Particles and LCC (c and f) Poly(St/NaSS) Particles on Bare Glass and APTMS-Modified Glass Substrates at 20 °C

	bare substrate			APTMS substrate		
value	a	b	c	d	e	f
ΔZ^a/nm	51 ± 2	66 ± 7	51 ± 5	53 ± 7	95 ± 3	43 ± 5
no. of particles per 10^3 nm	3.9	3.7	3.6	4.8	4.3	3.7
D^b/nm	256	269	278	209	235	267
$d_o - d^c$/nm	21	27	50	−26	−7	39

[a] Mean peak-to-valley distance. [b] Interparticle distance calculated from the particle number per 1.0 μm. [c] The interval between the particles, d_o = original particle diameter. A negative value indicates overlapping morphology due to the deformation.

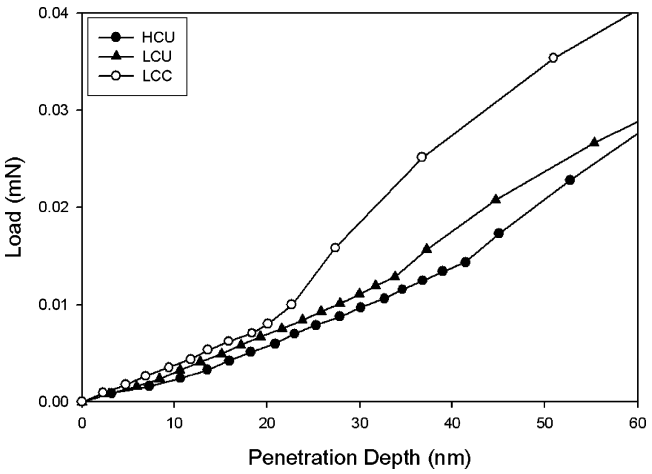

Figure 4. Load−displacement curves of the (●) HCU, (▲) LCU, and (○) LCC poly(St/NaSS) latex particles obtained from nanoindentation measurements with an applied load of 0.04 mN.

was injected at 90% conversion of the first stage polymerization. 0.1 wt % (based on styrene monomer) DVB was used as a cross-linker in the preparation of LCC latex particle. The prepared poly(St/NaSS) latexes were cleaned and purified using a serum replacement cell until the conductivity of the serum was the same as that of the DDI water.

Surface Modification of Glass Substrates. Glass microscope slides (Paul Marienfeld GmbH & Co.) were used as glass substrates (75 m × 25 mm with finely ground edges, precleaned). The slides were cleaned in a "piranha solution" (30% H_2O_2:98% H_2SO_4 = 1:3 v/v) at 120 °C for 1 h and then rinsed with distilled water, sonicated in methanol for 15 min, and dried under a N_2 atmosphere. The bare glass substrate was modified with APTMS to change its hydrophobicity. The slides were dipped in a 2 wt % APTMS methanol solution for 30 min, rinsed with 95% methanol aqueous solution and DI water, dried in a N_2 flush, and then cured in a vacuum oven at 120 °C for 1 h.

2- and 3-D Colloidal Crystal Arrays. For 2- and 3-D colloidal crystals, a natural convection drying method was applied. The purified latex (0.02 wt % solid) was deposited on a stainless steel (40 mm × 40 mm × 2 mm) plate with a circular tapered hole (diameter = 15 mm, taper angle = 60°) in its center, and the cell was allowed to dry in an incubator to form colloidal crystals at 20 °C. A detailed description of the drying cell was presented in our previous paper.[19]

Characterization. Characterization of Poly(St/NaSS) Latex Particles. Solid contents of the final latexes were determined by the gravimetric method. The solid contents of HCU, LCU, and LCC latexes were 7.8, 8.3, and 7.9 wt %, respectively. The average particle size and polydispersity were determined using capillary hydrodynamic fractionation (CHDF-2000, Matec Applied Science) and field-emission electron scanning microscopy (JSM-6500F, JEOL Co., Japan). The number-average particle size ($\overline{D_n}$) of HCU, LCU, and LCC latexes were found to be 235, 242, and 228 nm, respectively. The polydispersity index ($\overline{D_w}/\overline{D_n}$) was all at 1.007. The surface charge density was measured by a titration method using 0.02 M NaOH aqueous solution under N_2 gas.[22] The surface charge densities (σ) of the HCU, LCU, and LCC poly(St/NaSS) particles were calculated to be 38, 3, and 4 μC cm^{-2}, respectively. The properties of the HCU, LCU, and LCC latexes are listed in Table 1.

Elastic Modulus Measurement by Nanoindenter. A nanoindenter (MTS XP System, MTS Systems Corp.) was used to measure the mechanical properties of HCU, LCU, and LCC latex particles at 25 °C. In this experiment, a diamond Berkovich-type indenter tip was forced onto the sample being studied. The indentation depth is related to the area of contact between the indenter and the sample being tested. Multiple (five times) indentations were made at different locations on the particle surface at a fixed applied load. The load−displacement curves were recorded, from which the effective hardness and modulus values could be calculated.

Particle Array Patterns and Packing Densities of 2- and 3-D Colloidal Crystals. Morphology of the colloidal crystal arrays and crystal lattice patterns were observed using a field-emission scanning electron microscope (FE-SEM, JSM-6500F, JEOL Co., Japan). The packing density of the crystal was measured using a UV−vis spectrophotometer (UV-1601PC, Shimadzu Co., Japan). The UV−vis transmittance spectra of the crystals were obtained with an incident light perpendicular to the hexagonal closed packing regions. The APTMS substrate showed reproducible and high-quality spectra at all points, but the spectra from the bare substrate differed from spot to spot due to mixed structures of hcp and square lattices.

The crystal thickness was determined directly by measuring the intensity of the minimum of the UV−vis transmission spectra (i.e., the stop band) of the crystalline lattices assembled from the latex particles. All samples were dried, and the void spaces within the colloidal crystals were completely filled with air. The intensity of stop bands increases with layer number since scattering of diffusive light varies with the layer number of photonic crystals.[24] The intensity of the stop bands was linearly proportional to the crystal thickness when the number of (111) planes increased.

Image Analysis and Adhesion Force Measurement by Atomic Force Microscopy. The ordered 2-D array patterns of the poly(St/NaSS) latexes were obtained on a Digital Instruments IVa scanning probe microscope while the image heights were obtained using AFM tapping (noncontact) mode under ambient conditions. The *z*-axis profiles of the poly(St/NaSS) particle arrays on different glass substrates were obtained from sectional analysis of the surface profile of AFM images.

Adhesion force between poly(St/NaSS) latex particles and SiN_x or APTMS-modified SiN_x AFM tips respectively were measured using a Digital Instruments IVa scanning probe microscope by monitoring the force as a function of the displacement of the sample relative to the tip. The attraction (adhesion) force between the two is equal to the force needed to deflect elastically the cantilever during the jump to contact (or jump off contact). These forces are calculated by multiplying the appropriate cantilever deflection by its spring constant according to the Hooke's law. The spring constant of the tip used was 0.06 N/m.

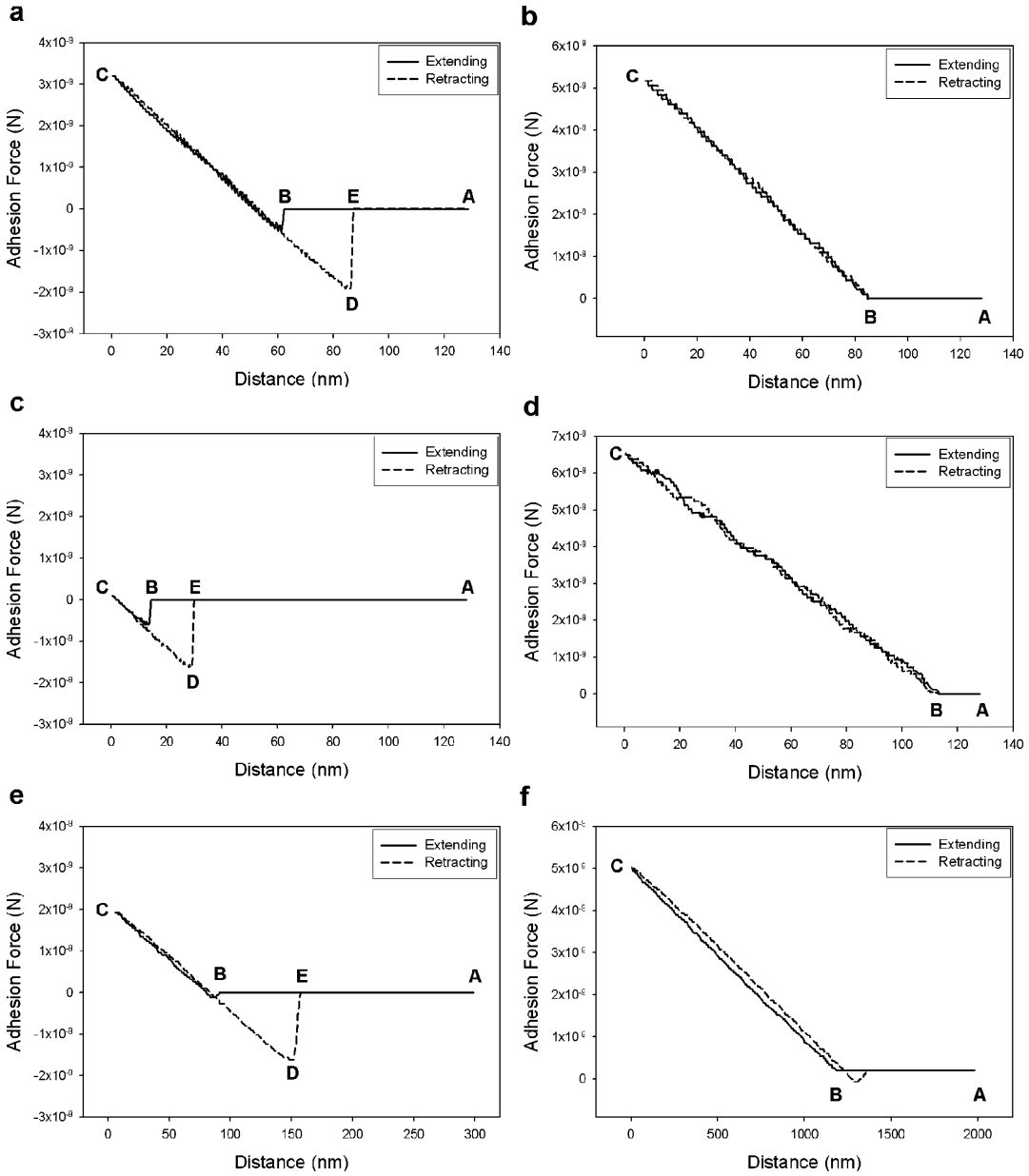

Figure 5. AFM adhesion force curves; (a, c, and e) between a SiN_x AFM tip and the surface of colloidal crystals of poly(St/NaSS) latex particles and (b, d, and f) between the APTMS-modified SiN_x AFM tip and the surface of the colloidal crystal of poly(St/NaSS) latex particles.

Table 3. Theoretical Adhesion Force (Attractive Interaction) for Two Media Interacting across Another Medium (a) Media 1:2:3 = Polystyrene:SiO_2:Water System and (b) Media 1:2:3 = Polystyrene:Hydrocarbon (C_3):Water System and the Measured Adhesion Force between Highly Charged HCU Poly(St/NaSS) Particle Surface and (a) SiN_x Tip and (b) APTMS-Modified SiN_x Tip

values		a	b
Hamaker constant (A_{132})[a]/J		8.98×10^{-21}	3.08×10^{-21}
adhesion force (calculated)/N	(i) sphere−surface[b]	-43.97×10^{-10}	-15.09×10^{-10}
	(ii) two spheres[c]	-21.98×10^{-10}	-7.55×10^{-10}
adhesion force (measured)/N	HCU poly(St/NaSS)	-19.11×10^{-10}	~0
	LCU poly(St/NaSS)	-16.33×10^{-10}	~0
	LCC poly(St/NaSS)	-16.14×10^{-10}	-2.75×10^{-10}

[a] A_{132} = Hamaker constants for two media interacting across another medium by Lifshitz theory. [b] The force law for sphere-planer surface geometry. [c] The force law for two interacting spheres geometry. Negative values indicate attraction (or adhesion) between two surfaces. The spring constant of the cantilever is 0.06 N/m.

Results and Discussion

Surface Morphology of Colloidal Crystals. Figure 1 shows the top view of the SEM micrographs of the monolayer and multilayer arrays of HCU on a bare (a and c) and APTMS-modified (b and d) glass substrates, respectively, at 20 °C.[19] The 2- and 3-D arrays from the APTMS-modified glass substrate showed dense packing pattern without crevices and were clearly deformed into a honeycomb shape (Figure 1b,d) as compared to those on the bare glass substrate (Figure 1a,c) with many line defects, dislocations, and crevices between ordered particles.

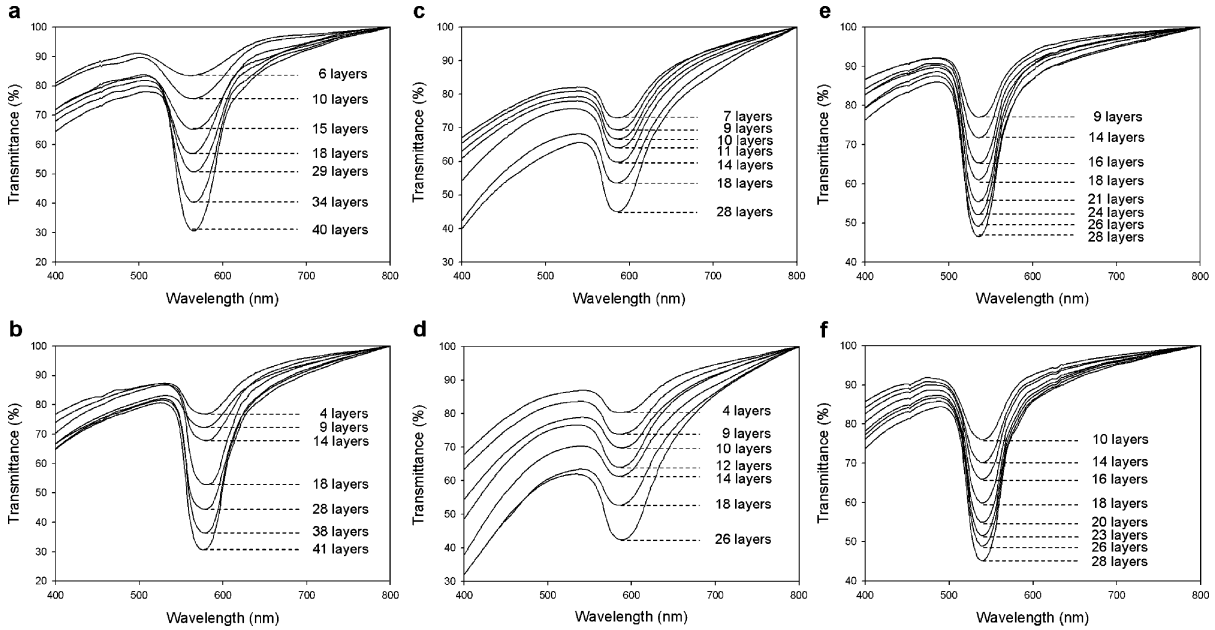

Figure 6. UV−vis transmission spectra taken at normal incidence to the (111) planes of cubic-close-packed lattices of HCU (a and b), LCU (c and d), and LCC (e and f) latex particles having different thicknesses on the cleaned, bare glass substrate (a, c, and e) and on the APTMS-modified glass substrate (b, d, and f).

This trend is also present in the multilayer array as shown in Figure 1d. The crystal lattices on the bare glass substrate showed both tetragonal and hexagonal close-pack (hcp or face-centered cubic, fcc) structures. However, very few tetragonal structures (square lattices) were found in the APTMS-modified glass samples (Figure 1, c vs d), except dislocations.

The FE-SEM micrographs of the top view of the mono- and multilayer cross-linked (LCC) poly(St/NaSS) particles arrays on the bare (Figure 2a−c) and APTMS-modified (Figure 2d−f) glass substrates at 20 °C reveal that the crystal lattice on the bare glass substrate showed both tetragonal and hexagonal close pack (hcp or face-centered cubic, fcc) structures, while very few tetragonal structures (square lattices) were found for those on the APTMS-modified glass substrate. The particle arrays on both substrates showed no discernible deformation, in contrast to the HCU particles adhered to the surface of the APTMS-modified glass substrate which were clearly deformed (Figure 1b). The hard LCC poly(St/NaSS) particles were not deformed despite possessing the right "free-slipping" conditions for adhesional deformation.

AFM Surface Profile Analyses. The AFM surface profiles of the outermost multilayer of the three latexes (HCU, LCU, and LCC) on the bare (Figure 3a−c) and APTMS-modified glass (Figure 3d−f) substrates show that for latexes HCU and LCU deposited on APTMS-modified glass substrates the distance between the particles (d) was shorter. This shows a close packing of the particles as they came into contact with each other. From the peak-to-valley profiles in Figure 3 and the measured values, d or $d_o - d$ in Table 2, it is evident that the un-cross-linked latexes, HCU and LCU, on the APTMS-modified glass were more densely and closely packed comapred with those on the bare glass substrate, while the deformations in the z-direction (ΔZ) were insignificant. This means that particle deformation in packed arrays depends not only on the surface nature of the substrate but also on the surface charge density of the particles. The former provides the "free-slipping" conditions while the latter relates to the degree of hydration and particle interaction. The APTMS coating offered a soft "grasslike" substrate surface that could be deformed by the hydrated hairy poly(St/NaSS) particles to provide a greater contact area.[25−27] This together with the hairy structure on the surface of the particles gave rise to smaller interstices between the particle and the APTMS surface. The resulting larger capillary force at the water meniscus in the interstices that ensued caused adhesional deformation of the hydrated particles during natural convection drying. "Incoming" HCU and LCU particles easily attached closely to the nuclei on the APTMS layer without anchoring onto the peripheral surface and adhesional deformation occurred as water evaporated.[19]

The arrays of cross-linked particle (LCC) on the APTMS surface were not deformed at all and were similar to that on the bare glass surface, despite strong capillary force was also experienced by these particles. This could be explained by the higher elastic modulus of these hard partilces measured with the Berkovich indenter compared to those of HCU and LCU latexes. The load−displacement curves on the nanoindentation for three latex types are given in Figure 4. It can be seen that the penetration increased with load for each latex type. At any constant penetration depth, the load was in the order LCC > LCU > HCU. In fact, the load for LCC was the largest over the whole penetration range studied and increased very rapidly at high penetration.

Capillary Forces and Elastic Modulus. From the Young−Laplace equation ($\Delta P = 2\gamma/R$) for spherical surfaces, the capillary pressure (ΔP) induced at the water meniscus in the interstices (R) during natural convection drying was 0.0033 GPa, using $\gamma = 72.8$ mJ/m^2 and $R = 43.68$ nm from the cross-sectional SEM analysis. However, the elastic modulus for LCC particles at 0.0037 GPa was higher than its ΔP and also the elastic moduli of the un-cross-linked HCU (at 0.0022 GPa) and LCU at 0.0025 GPa at a constant penetration depth of 50 nm where the unit area (S) = 9.41×10^6 nm^2. Thus, it is clear that the hard LCC particles could not be deformed because of its high elastic modulus.

During thermal annealing of polymeric microspheres above the glass transition temperature, the spherical contour of the individual particles are deformed to a polyhedral structure if they are film-forming.[28] The peak-to-valley heights (ΔZ) of the

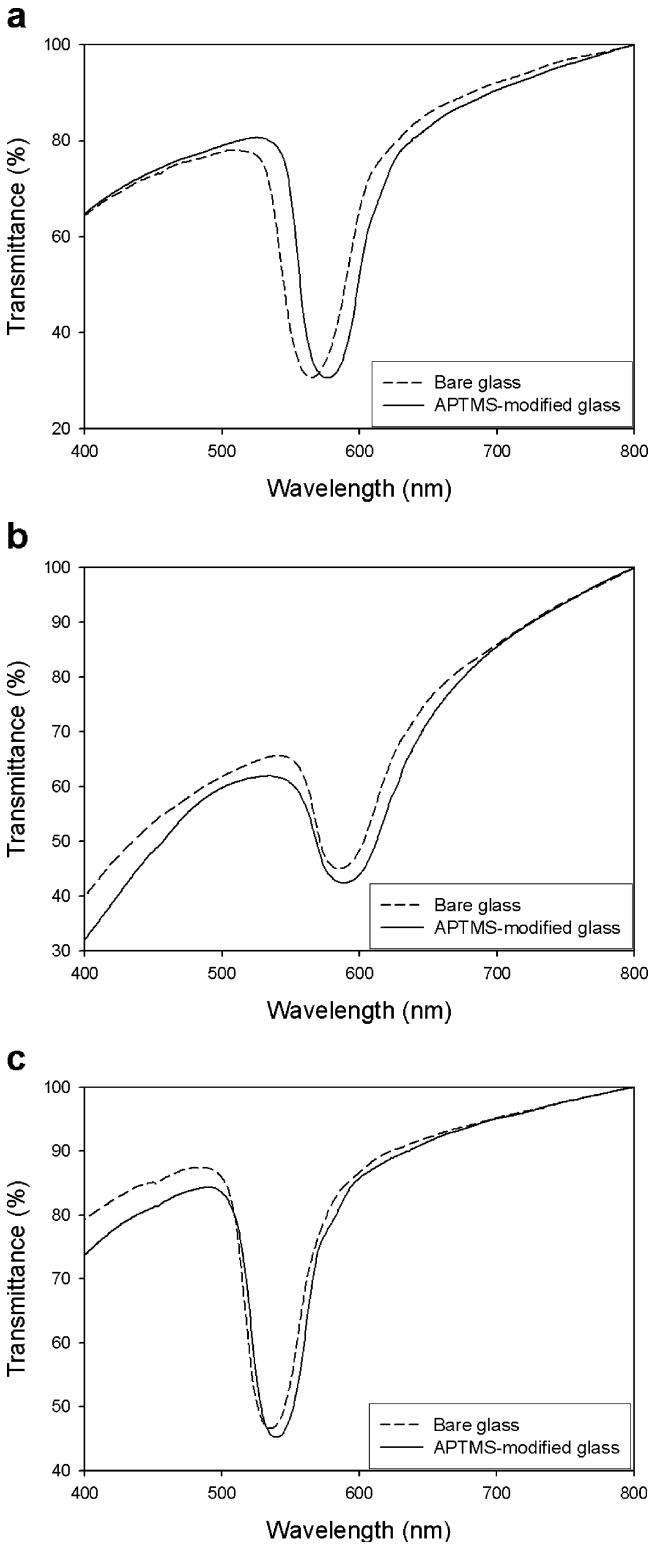

Figure 7. Comparison of the wavelengths at the minimum transmittance obtained from UV−vis transmission spectra of cubic-close-packed lattices of (a) HCU, (b) LCU, and (c) LCC latex particles on cleaned, bare glass substrate (dotted line) and on APTMS-modified glass substrate (solid line).

closely packed particles would decrease. Our results on the poly(St/NaSS) particles showed little changes in ΔZ, indicating clearly no deformation of the particles and hence no film formation of the colloidal crystals during drying.

Adhesion Force between Latex Particles and Substrates by AFM. To show that the APTMS layer fulfils the free-slipping condition, the attractive force between the surface of the latex particles and the APTMS layer was measured indirectly (i.e., not in the wet state) using an AFM with either an APTMS-modified SiN_x AFM tip or a SiN_x AFM tip, as shown in Figure 5. It was found that the attractive force between the APTMS-modified SiN_x AFM tip, and the surfaces of the three different latex particles (Figure 5b,d,f) were negligible compared with those between a SiN_x AFM tip and the latexes (Figure 5a,c,e). For example, the measurement began at point A where the SiN_x tip and the surface of the HCU particle were far from each other (Figure 5a). From point B the SiN_x tip started to experience the London−van der Waals attractive interaction, resulting in a slight dip at point B where the SiN_x tip and the surface of the HCU particle came "into contact". On retraction, the SiN_x tip did not separate from the HCU particle but remained in contact from point C to D. At point D, the SiN_x tip and the surface of the HCU particle suddenly jumped apart, and the hysteresis between points D and E is a direct measurement of the adhesion force. There was no hysteresis between the APTMS-modified SiN_x tip and the surface of the latex particle, and hence there was no attractive interaction between them (Figure 5a,c,e). These results are in accordance with the "free-slipping" theory proposed by Nagayama et al.[29] They are strong evidence that defect-free colloid crystals can be formed on the smooth substrate surface because the particles are able to slip on the

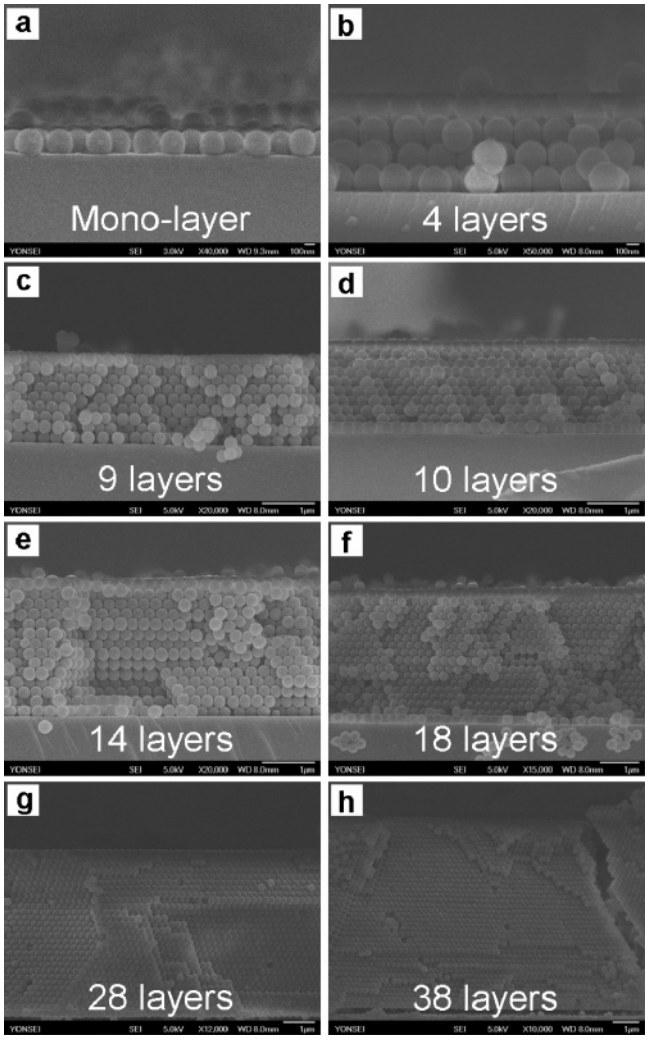

Figure 8. SEM micrographs of the interior of the colloidal crystals at different thicknesses (number of layers) of the LCC poly(St/NaSS) latex particles on cleaned, bare glass substrate.

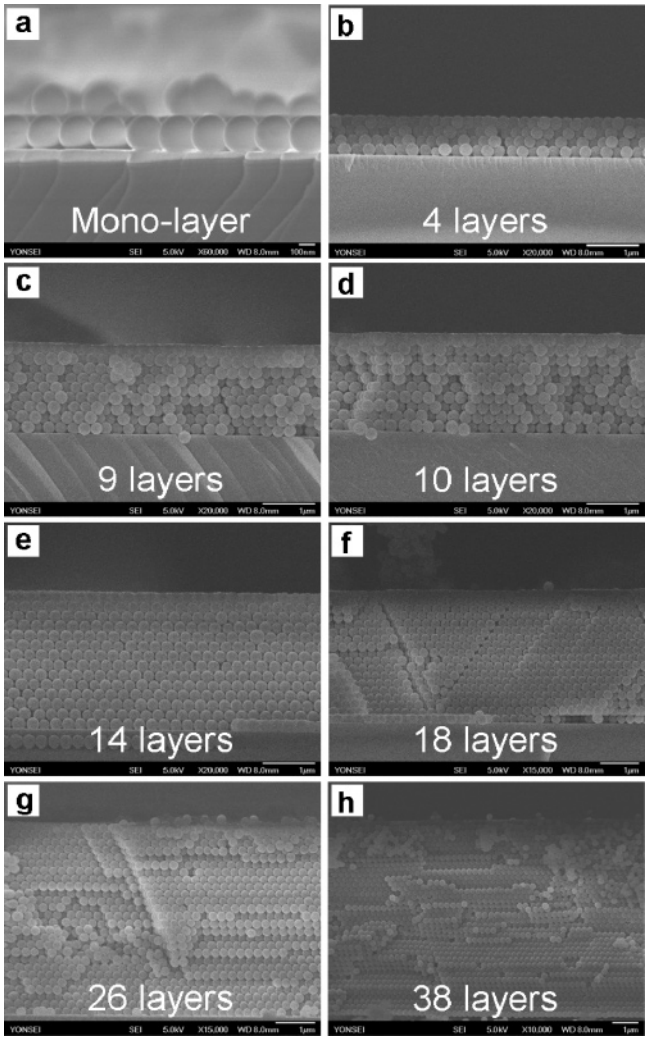

Figure 9. SEM micrographs of the interior of the colloidal crystals at different thicknesses (number of layers) of the LCC poly(St/NaSS) latex particles on APTMS-modified glass substrate.

soft "grasslike" APTMS-modified substrate surface. Similar behavior was observed for all the three latexes, HCU, LCU, and LCC. The measured attractive forces for each sample are listed in Table 3.

Lifshitz Attractive Forces. Table 3 also shows the theoretical adhesion forces (F_A) calculated for two interacting media across a third medium for two geometries consisting of (i) a hard sphere and a hard planar surface and (ii) two spheres with the appropriate Hamaker constants (A_{132}) given by

$$\text{(i) } F_A = -\frac{A_{132}R}{6D^2}, \quad \text{(ii) } F_A = -\frac{A_{132}R}{12D^2} \tag{1}$$

where R is the sphere radius, A_{132} is the Hamaker constants for two media interacting across another medium, and D is the distance between two bodies of different geometries. To calculate F_A for two bodies of different geometries in contact (adhesion), the cutoff distance (D) was assumed to be 0.2 nm. To compute the appropriate Hamaker constant (A_{132}) using the Lifshitz theory, it is necessary to know the values of the Hamaker constants for (a) polystyrene−polystyrene interaction across water (A_{131}) and silica−silica interaction across water (A_{232}) and (b) polystyrene−polystyrene interaction across water (A_{131}) and hydrocarbon−hydrocarbon interaction across water (A_{232}). Here, the values of (a) $A_{131} = 9.5 \times 10^{-21}$ J and $A_{232} = 8.5 \times 10^{-21}$ J and (b) $A_{131} = 9.5 \times 10^{-21}$ J and $A_{232} = 1.0 \times 10^{-21}$ J were used,[30] which were obtained from the Lifshitz calculations based on the latest interpretation of dielectric data.[31] From these data, the Hamaker constant (A_{132}) between latex particle surface and SiN_x AFM tip is (a) 8.98×10^{-21} J, and that between latex particle surface-APTMS-modified SiN_x AFM tip is (b) 3.08×10^{-21} J.

Table 3 shows that the calculated adhesive forces for interaction between two hard-sphere geometry are in close agreement with the adhesive forces measured using a SiN_x AFM tip on the latex particle surface. In contrast, the calculated adhesive forces based on the two hard spheres geometry were much lower between latex particle surface and APTMS-modified surface compared to those obtained with the silica surface. The Lifshitz calculations indicate some residual attraction between latex particles and substrate surfaces while no adhesion was revealed by the AFM measurement using the APTMS-modified SiN_x tip. From the theoretically calculated adhesive forces which are closely corroborated by the actual measurement using the AFM technique, we believe we have obtained a fairly good approximation of the forces interacting between the particles and the substrate. Thus, it may be concluded that there was near absence of adhesion between the latex particles on APTMS-modified SiO_2 substrate in the wet state. Thus, the incoming particles can move easily and attach closely to preformed nuclei on the APTMS layer. Without scattered anchoring onto the substrate surface, dense packing of the particles is favored and almost defect-free colloidal crystals are formed.

Colloidal Crystal Thickness and Packing Density. Figure 6 shows the transmission spectra recorded at normal incidence to the (111) planes for the colloidal crystals of HCU, LCU, and LCC on two different substrates at different crystal thickness. The wave lengths at the minimum of the transmission were $\lambda_{(HCU)} = 565$ nm, $\lambda_{(LCU)} = 585$ nm, $\lambda_{(LCC)} = 535$ nm on the bare glass substrate and $\lambda_{(HCU)} = 579$ nm, $\lambda_{(LCU)} = 589$ nm, $\lambda_{(LCC)} = 539$ nm on the APTMS-modified glass substrate. These wavelengths were independent of the crystal thickness. A well-ordered crystal structure of the particle array on the APMTS-modified substrate is to be expected since the stop-band width of the colloidal crystals on APTMS-modified substrate was narrower than that on the bare glass substrate. This was, however, broader than the theoretical values calculated by DLS theory or the Korringa−Kohn−Rostoker (KKR) model.[24] This implies some polycrystalline colloidal crystal are present. The APTMS layer prevented "pinning" of the particle, important in reducing point and line defects. However, simultaneous multinucleation was inevitable in the horizontal-type array cells used, and this may lead to some polycrystalline crystals and dislocations. Though multinucleation happened on the bare and APTMS-modified glass substrates, the colloid crystals on the APTMS-modified glass substrate showed better packing density without square lattice structure considered as bulky defect.

The wavelengths (λ) at the minimum transmission of the colloidal crystals were $\lambda_{(HCU)} = 579$ nm, $\lambda_{(LCU)} = 589$ nm, and $\lambda_{(LCC)} = 539$ nm on the APTMS-modified glass substrate. Assuming an ideal colloidal crystal composing entirely of the fcc (or hcp) structure, λ have been calculated to be $\lambda_{(HCU)} = 565$ nm, $\lambda_{(LCU)} = 584$ nm, and $\lambda_{(LCC)} = 535$ nm using the Bragg's diffraction equation

$$m\lambda = 2d_{hkl}(n_c^2 - \sin^2\theta)^{1/2} \tag{2}$$

where m is an integer, n_c the refractive index of the crystalline assembly calculated from the interstitial void of hexagonal

closed packing (0.26) and the reflective indices of air (1.00) and polystyrene (1.59), d_{hkl}, $(2/3)^{0.5}d_0$ (the grating constant) for the (111) fcc plane, and the angle of incident light, 0°.[3,32] The difference between the observed and calculated λ probably arose from the value of packing density used. The packing density of the colloid crystals on the APTMS-modified substrate was calculated as 0.80, 0.76, and 0.76 using Bragg's equation, assuming that the d_{111} for APTMS was the same as the above ideal value, since the ΔZ difference was found to be negligible (see Table 2). As seen in Figure 7, the difference between the λ values on the bare glass and APTMS-modified glass substrates, resulting from the adhesional deformation of the particles, was 14 nm for HCU colloidal crystals and, however, only 5 and 4 nm for LCU and LCC colloidal crystals. The data indicates that the degree of adhesional deformation of the HCU particles was higher than that of the LCU particles because of its higher surface charge density. In the case of LCC particles, there was no adhesional deformation of the particles because of its high cross-linking density and elastic modulus.

Interior Structure of Colloidal Crystals by SEM. The FE-SEM micrographs show cross-sectional interior views of the 2- and 3-D arrays from the LCC latex particles on bare glass substrate (Figure 8) and on APTMS-modified (Figure 9) glass substrate. The micrographs were captured at 90° tilt angle. In the case of the un-cross-linked particles as shown in our previous work,[19] the crystal lattice on APTMS-modified glass substrate showed a honeycomb-like hexagonal packing structure, and one could see deformation of the particle shape to achieve dense packing regardless of the number of crystal layers (up to 38 layers). In the case of LCC latex particles as seen in Figure 9, densely packed arrays without particle deformation was observed on APTMS-modified glass substrate. This result was corroborated by the top-view SEM images of the 2- and 3-D colloidal crystals on the different glass substrates shown in Figure 2.

Conclusions

The 2- and 3-D colloidal arrays were fabricated using three different types of monodisperse poly(St/NaSS) particles (HCU, LCU, and LCC) on APTMS-modified glass substrates at 20 °C. The packings of the HCU and LCU poly(St/NaSS) particles formed on the APTMS-modified glass surface were found to be a square-lattice-free hcp structure. For HCU and LCU latex particles, the distance between the un-cross-linked poly(St/NaSS) particles was reduced when the particles were deposited on APTMS-modified glass substrates due to adhesional deformation. This packing pattern was attributed to "free slipping" of latex particles into colloidal crystal nuclei. The "free slipping" condition prevented scattered anchoring of incoming particles onto the substrate and allowing smaller interstices between particles to be formed, leading to a stronger capillary force that deformed the particles. However, adhesional deformation of the LCC particles was not observed on the APTMS-modified glass substrate due to its high cross-linking density (92.8%). The high elastic modulus of LCC resisted adhesion deformation arising from the capillary force and remained separated.

Only a negligible attractive force existed between the APTMS substrate and the poly(St/NaSS) particles. There was no substantial adhesion between the poly(St/NaSS) particle surface and the APTMS-modified SiO_2 substrate in the wet state. The adhesion force measured between the APTMS-modified SiN_x tip and the self-assembled particle arrays presented a direct correlation with the hydrophobicity of the substrate and was in reasonable agreement with values calculated from adhesion force theory employing appropriate Hamaker constants.

The present findings show a method that is potentially useful in fabricating high-quality photonic crystal with full band-gap properties (i.e., the exact attenuation of a stop band).

Acknowledgment. This work was financially supported by the Ministry of Education and Human Resources Development (MOE), the Ministry of Commerce, Industry and Energy (MOCIE), and the Ministry of Labor (MOLAB) through fostering project of the Lab of Excellence. This work was supported by Ministry of Commerce, Industry, and Energy (MOCIE) through the project of NGNT (Nos. 10024146 and 10024260). This work was also supported by the Korea Science and Engineering Foundation (KOSEF) grant funded by the Korea government (MOST) (No. R11-2007-050-02001-0). This work had been supported by the Korea Research Foundation Grant funded by the Korean Government (MOEHRD, R08-2003-000-11116-0).

References and Notes

(1) Xia, Y.; Gates, B.; Yin, Y.; Lu, Y. *Adv. Mater.* **2000**, *12*, 693−713.
(2) Alfrey, T., Jr.; Bradford, E. B.; Vanderhoff, J. W.; Oster, G. *J. Opt. Soc. Am.* **1954**, *44*, 603−9.
(3) Goldenberg, L. M.; Wagner, J.; Stumpe, J.; Paulke, B. R.; Gornitz, E. *Mater. Sci. Eng., C* **2002**, *C22*, 233−237.
(4) Velev, O. D.; Jede, T. A.; Lobo, R. F.; Lenhoff, A. M. *Chem. Mater.* **1998**, *10*, 3597−3602.
(5) Yablonovitch, E.; Gmitter, T. J. *Phys. Rev. Lett.* **1989**, *63*, 1950−3.
(6) Ye, Y.-H.; LeBlanc, F.; Hache, A.; Truong, V.-V. *Appl. Phys. Lett.* **2001**, *78*, 52−54.
(7) Park, S. H.; Xia, Y. *Langmuir* **1999**, *15*, 266−273.
(8) Bevan, M. A.; Lewis, J. A.; Braun, P. V.; Wiltzius, P. *Langmuir* **2004**, *20*, 7045−7052.
(9) Jiang, P.; Hwang, K. S.; Mittleman, D. M.; Bertone, J. F.; Colvin, V. L. *J. Am. Chem. Soc.* **1999**, *121*, 11630−11637.
(10) Distler, D.; Kanig, G. *Colloid Polym. Sci.* **1978**, *256*, 1052−60.
(11) Goh, M. C.; Juhue, D.; Leung, O. M.; Wang, Y.; Winnik, M. A. *Langmuir* **1993**, *9*, 1319−22.
(12) Campbell, M.; Sharp, D. N.; Harrison, M. T.; Denning, R. G.; Turberfield, A. J. *Nature (London)* **2000**, *404*, 53−56.
(13) van Blaaderen, A.; Rue, R.; Wiltzius, P. *Nature (London)* **1997**, *385*, 321−324.
(14) Egen, M.; Zentel, R. *Chem. Mater.* **2002**, *14*, 2176−2183.
(15) Kralchevsky, P. A.; Denkov, N. D. *Curr. Opin. Colloid Interface Sci.* **2001**, *6*, 383−401.
(16) Kralchevsky, P. A.; Nagayama, K. *Langmuir* **1994**, *10*, 23−36.
(17) Paunov, V. N.; Kralchevsky, P. A.; Denkov, N. D.; Nagayama, K. *J. Colloid Interface Sci.* **1993**, *157*, 100−12.
(18) Velev, O. D.; Denkov, N. D.; Paunov, V. N.; Kralchevsky, P. A.; Nagayama, K. *Langmuir* **1993**, *9*, 3702−9.
(19) Lee, J. M.; Kim, J. H.; Ho, C. C.; Cheong, I. W. *Polymer* **2007**, *48*, 4804−4813.
(20) Butt, H.-J. *J. Colloid Interface Sci.* **1994**, *166*, 109−17.
(21) Xiao, X.; Qian, L. *Langmuir* **2000**, *16*, 8153−8158.
(22) Cheong, I. W.; Kim, J. H. *Colloid Polym. Sci.* **1997**, *275*, 736−743.
(23) Cheong, I.-W.; Kim, J.-H. *Colloids Surf. A* **1999**, *153*, 137−142.
(24) Gates, B.; Lu, Y.; Li, Z. Y.; Xia, Y. *Appl. Phys. A* **2003**, *76*, 509−513.
(25) Ostrowska, J.; Narebska, A. *Colloid Polym. Sci.* **1983**, *261*, 93−8.
(26) Thun, C.; van de Ven, T. G. M. *Colloids Surf. A* **1998**, *145*, 205−212.
(27) Wu, X.; van de Ven, T. G. M. *Langmuir* **1996**, *12*, 3859−3865.
(28) Lee, D.-Y.; Choi, H.-Y.; Park, Y.-J.; Khew, M.-C.; Ho, C.-C.; Kim, J.-H. *Langmuir* **1999**, *15*, 8252−8258.
(29) Denkov, N.; Velev, O.; Kralchevski, P.; Ivanov, I.; Yoshimura, H.; Nagayama, K. *Langmuir* **1992**, *8*, 3183−90.
(30) Bergstrom, L. *Adv. Colloid Interface Sci.* **1997**, *70*, 125−169.
(31) Roth, C. M.; Lenhoff, A. M. *J. Colloid Interface Sci.* **1996**, *179*, 637−639.
(32) Cong, H.; Cao, W. *Langmuir* **2004**, *20*, 8049−8053.

MA702283A